ORIGINAL RESEARCH

OLA1 Phosphorylation Governs the Mitochondrial Bioenergetic Function of Pulmonary Vascular Cells

Paul Sidlowski[1,2,3,4], Amanda Czerwinski[1,2,3,4], Yong Liu[5], Pengyuan Liu[5], Ru-Jeng Teng[1,2,3,4], Suresh Kumar[2,4], Clive Wells[6], Kirkwood Pritchard, Jr.[2,3,4,7], Girija G. Konduri[1,2,3,4], and Adeleye J. Afolayan[1,2,3,4]

[1]Department of Pediatrics, [2]Cardiovascular Research Center, [3]Children's Research Institute, [4]Department of Pathology, [5]Department of Physiology, [6]Department of Cell Biology, Neurology, and Anatomy, and [7]Department of Surgery, Medical College of Wisconsin, Wauwatosa, Wisconsin

ORCID ID: 0000-0001-9886-6694 (A.J.A.).

Abstract

Mitochondrial function and metabolic homeostasis are integral to cardiovascular function and influence how vascular cells respond to stress. However, little is known regarding how mitochondrial redox control mechanisms and metabolic regulation interact in the developing lungs. Here we show that human OLA1 (Obg-like ATPase-1) couples redox signals to the metabolic response pathway by activating metabolic gene transcription in the nucleus. OLA1 phosphorylation at Ser232/Tyr236 triggers its translocation from the cytoplasm and mitochondria into the nucleus. Subsequent phosphorylation of OLA1 at Thr325 effectively changes its biochemical function from ATPase to GTPase, promoting the expression of genes involved in the mitochondrial bioenergetic function. This process is regulated by ERK1/2 (extracellular-regulated kinases 1 and 2), which were restrained by PP1A (protein phosphatase 1A) when stress abated. Knockdown of ERK1 or OLA1 mutated to a phosphoresistant T325A mutant blocked its nuclear translocation, compromised the expression of nuclear-encoded mitochondrial genes, and consequently led to cellular energy depletion. Moreover, the lungs of OLA1 knockout mice have fewer mitochondria, lower cellular ATP concentrations, and higher lactate concentrations. The ensuing mitochondrial metabolic dysfunction resulted in abnormal behaviors of pulmonary vascular cells and significant vascular remodeling. Our findings demonstrate that OLA1 is an important component of the mitochondrial retrograde communication pathways that couple stress signals with metabolic genes in the nucleus. Thus, phosphorylation-dependent nuclear OLA1 localization that governs cellular energy metabolism is critical to cardiovascular function.

Keywords: pulmonary hypertension; pulmonary vascular cells; phosphorylation; OLA1; mitochondrial energy metabolism

Clinical Relevance

Decreases in mitochondrial biogenesis and function accompany cardiovascular diseases. Our studies demonstrated that the Thr(T325) phosphorylation form of OLA1 (Obg-like ATPase-1) determines the mitochondrial content and function of vascular endothelial cells.

(Received in original form May 6, 2022; accepted in final form December 8, 2022)

Supported partly by National Institutes of Health grants (National Heart, Lung, and Blood Institute grant 5 K08 HL133379-05, Children's Hospital of Wisconsin Research Institute, and Department of Pediatrics at the Medical College of Wisconsin).

Author Contributions: Conception and design: P.S. performed animal studies, DNA biotinylation, DNA binding assays, RT-qPCR, and ATP/GTPase assays; A.C. performed mitochondrial isolation, mouse lung cell isolation, and chronic hypoxia experiments; C.W. performed transmission EM and analysis; S.K. performed confocal microscopy and image analyses; A.J.A. performed IP, IB, and data analysis; P.L. performed chromatin IP with high-throughput DNA sequencing analysis; Y.L. performed RNA sequencing analysis. Studies, data collection, and data analysis: P.S., C.W., P.L., Y.L., S.K., R.-J.T., G.G.K., and A.J.A. Drafting manuscript for important intellectual content: P.S., A.C., K.P., S.K., R.-J.T., G.G.K., and A.J.A. Proofing and final draft: P.S., A.C., C.W., K.P., P.L., Y.L., R.-J.T., G.G.K., and A.J.A.

Data availability: The next-generation sequencing data generated in this study have been submitted to the Gene Expression Omnibus database under accession numbers GSE134510, GSE146557, and GSE146648. In addition, the data from the MS (mass spectrometry) analysis were deposited in the Proteome Standard Repository/Database under accession numbers JPST000666/PXD015191 and JPST000757/PXD017707.

Correspondence and requests for reprints should be addressed to Adeleye J. Afolayan, M.D., Associate Professor of pediatrics, Division of Neonatology, Suite C410, 999 North 92nd Street, Wauwatosa, WI 53226. E-mail: aafolaya@mcw.edu.

This article has a related editorial.

This article has a data supplement, which is accessible from this issue's table of contents at www.atsjournals.org.

Am J Respir Cell Mol Biol Vol 68, Iss 4, pp 395–405, April 2023

Originally Published in Press as DOI: 10.1165/rcmb.2022-0186OC on December 8, 2022
Internet address: www.atsjournals.org

Proper functioning of mitochondria is central to cellular homeostasis and organismal health. Thus, diverse signaling mechanisms respond to altered mitochondrial function to prevent cell death when various sensor molecules activate transcription factors or cofactors that regulate metabolic stress responses (1–6). In return, mitochondria respond to nuclear commands by feeding information back to the nucleus that modifies or regulates gene expression patterns, thereby restoring cellular homeostasis (6). Central to these processes are mitochondria that sense and integrate stress signals into the nucleus (1, 7, 8). Thus, the nucleus's decision to maintain health or promote disease critically depends on responses initiated locally within mitochondria.

Cells use diverse protein kinases for dynamic two-way communication between mitochondria and the nucleus (5, 9, 10). Several kinases and phosphatases that add or remove a phosphate group to or from protein targets are ubiquitously expressed in mammalian cells (11). Notably, ERK1/2 (extracellular-regulated kinases 1 and 2), which are ubiquitously expressed, are stress responders. Activating ERK1/2 through phosphorylation induces signaling cascades within the cell to promote cellular homeostasis (12, 13). To prevent overactivation, these kinases are inactivated by protein phosphatases that dephosphorylate them or their protein targets. Hence, cells adapt to and resist stress by preserving the number, integrity, and function of mitochondria through intricate cross-talk among signaling pathways, kinases, and phosphatases (14).

Human OLA1 (Obg-like ATPase-1) belongs to a large family of GTPases belonging to the TRAFAC (translation factor) class and YchF subfamily (15). Although it is a member of the GTPase family, OLA1 can hydrolyze ATP and GTP (15). The protein is ubiquitously expressed in all tissues, including pulmonary artery endothelial cells (PAECs) and smooth muscle cells (16). The OLA1 protein consists of a central guanidine domain flanked by a coiled-coil ATPase domain and a C-terminal TGS (17). Although its function in cell biology is mostly uncharacterized, OLA1 is involved in DNA repair, tumorigenesis, cell cycle regulation, and cellular stress response to oxidative and heat stresses (16, 18–21). Not surprisingly, aberrant OLA1 expression is detected in human cancers, and its expression positively correlates with tumor progression (22–24). Importantly, it has been reported that OLA1 in tumor cells promotes mitochondrial energy metabolism by interacting with ZFAS1 (ZNFX1 antisense RNA 1), a long-coding RNA, and increases glycolysis by downregulating the expression of enzymes involved in oxidative phosphorylation (22). Accordingly, knocking OLA1 down reduces glycolysis and tumor progression (25). Contrarily, despite many similarities, persistent pulmonary hypertension of the newborn (PPHN) is not a sheer mimic of cancer but exhibits unique characteristics. For example, decreased pulmonary OLA1 expression is reported in patients with PPHN. Furthermore, unlike in tumor cells, knocking OLA1 down in vascular cells increases glycolysis and cell death (16). One plausible explanation for this dichotomous behavior is that the biochemical function that enables the protective function of OLA1 in vascular cells

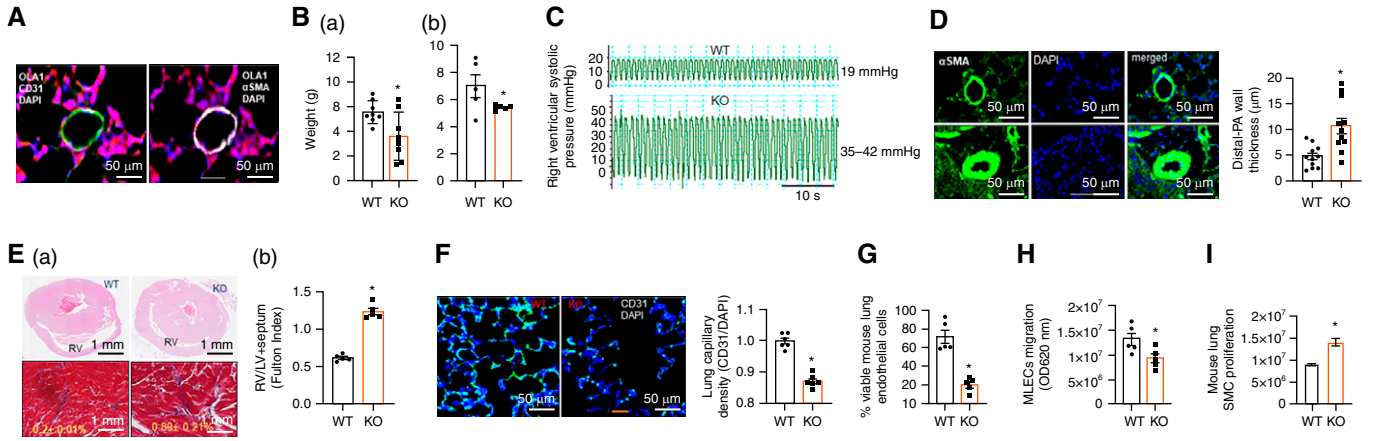

Figure 1. OLA1 (Obg-like ATPase-1) deletion precipitates cardiopulmonary remodeling. (*A*) Representative images of lung sections immunostained with anti-OLA1 antibodies, anti-CD31 antibodies, anti-αSMA (α-smooth muscle actin) antibodies and counterstained with DAPI in female wild-type (WT) mice killed on P7 (scale bar, 50 μm). (*Ba* and *Bb*) Bar charts of mouse weight in grams on P7: (*Ba*) WT versus knockout (KO), male ($n = 8$), and (*Bb*) WT versus KO, female ($n = 5$), killed on P7. *$P < 0.0001$ (Student's *t* test). (*C*) Representative tracing of right ventricular (RV) pressure over time in WT mice and *Endo*-OLA1$^{-/-}$ mice (male) on P7 ($n = 5$). *$P < 0.0002$ (Student's *t* test). (*D*) Representative images of lung sections immunostained with anti-αSMA antibodies and counterstained with DAPI showing small PAs in WT mice (upper panels) and Endo-OLA1 KO mice (lower panels) (male) killed on Day 10 (scale bar, 50 μm; $n = 5$). *$P < 0.0001$ (Student's *t* test). (*Ea*) Representative images of heart sections stained with hematoxylin and eosin (upper panels) and Masson's trichome (lower panels) from WT mice and Endo-OLA1 KO mice (scale bar, 1 mm). The number represents the percentage of interstitial fibrosis ($n = 3$, male, killed on P7). (*Eb*) Bar chart plots of the weight of the RV wall normalized to the weight of the LV plus the interventricular septum (Fulton index) (male, $n = 5$). *$P < 0.0001$ (Student's *t* test). (*F*) Representative images of lung sections stained with anti-CD31 and counterstained with DAPI (scale bar, 50 μm). Bar chart depicts the ratio of CD31 to DAPI signal intensity in 10 areas of the lungs ($n = 4$, male, on P7). *$P < 0.005$. Data are expressed as mean ± SEM, and statistical significance was assessed using one-way ANOVA. (*G* and *H*) Bar charts showing viability (*G*) and migration (*H*) of MLECs isolated from male WT mice and *Endo*-OLA1 KO mice (P7, $n = 5$). *$P < 0.001$ (*G*) and $P < 0.002$ (*H*) (Student's *t* test). (*I*) Bar chart showing proliferation in mouse lung microvascular SMCs from WT mice and Endo-OLA1 KO mice ($n = 5$). *$P < 0.00321$ (Student's t test). LV = left ventricle; MLEC = mouse lung microvascular endothelial cell; OD260nm = optical density at 260 nm; P7 = Postnatal Day 7; PA = pulmonary artery; SMC = smooth muscle cell.

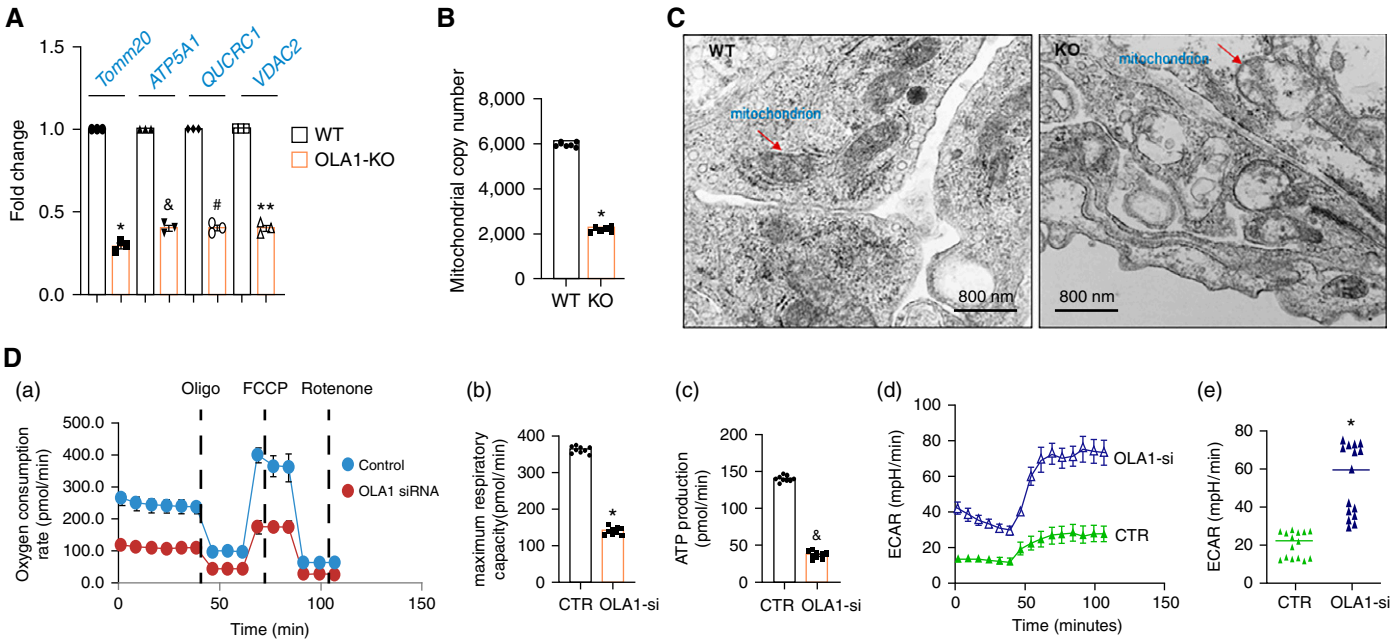

Figure 2. OLA1 deletion decreases the mitochondrial bioenergetic function of vascular cells. (*A*) Bar chart showing mRNA concentrations of select nuclear-encoded mitochondrial genes (*Tomm20* [translocase of outer mitochondrial membrane 20], *VDAC2* [voltage-dependent anion channel 2], *QUCRC1*, and *ATP5A1*) in WT mice and Endo-OLA1 KO lungs. GAPDH and 18S were used as housekeeping genes ($n=6$). Fold changes are expressed as mean ± SEM, and statistical significance was assessed using two-way ANOVA. $^{*}P<0.0001$, $^{\&}P<0.0001$, $^{\#}P<0.0001$, and $^{**}P<0.0001$. (*B*) Bar chart showing mitochondrial copy numbers in WT mice and Endo-OLA1 KO lungs (male, killed on P7). BECN1 (beclin 1) and NEB (nebulin) (nuclear) gene expression concentrations were normalized against concentrations of TrLEV and 12S (mitochondrial) genes ($n=5$). Data are expressed as mean ± SEM, and statistical significance was assessed using 2-way ANOVA. $^{*}P<0.0001$. (*C*) Representative ultrastructural images of mitochondria in endothelial cells from WT mice and Endo-OLA1 KO lung (male, killed on Postnatal Day 9). The orange arrows point to a mitochondrion. An AMT NanoSprint 12 camera system was used, with exposure for 2,000 ms × 2 SD (gain = 1, bin = 1) (scale bar, 800 nm; direct magnification of 25,000). (*D*) Graph of oxygen consumption of human neonatal pulmonary artery endothelial cells (PAECs) and PAECs transfected with siRNAs targeting native OLA1. Data represents oxygen consumption in 20,000 over time after cell treatment with oligomycin, FCCP, and rotenone ($n=4$). Data were corrected against protein concentrations measured using bicinchoninic acid assay. Data are expressed as mean ± SEM, and statistical significance was assessed using a two-sided unpaired Student's *t* test. (*Da* and *Db*) Scatter plots of maximum respiratory capacity (pmol/min in normal PAECs and OLA1 depleted PAECs, $n=3$, 10 data points were plotted $^{*}P<0.0001$, Student's *t* test. *D*(*c*) scatter plots of ATP production in normal PAECs and OLA1-depleted PAECs ($n=3$, 10 data point per sample, $^{\&}P<0.00005$, Student's *t* test. (*Dc* and *Dd*) Graph (*Dc*) and bar chart (*Dd*) of extracellular acid production in normal PAECs and OLA1-depleted PAECs ($n=4$) $^{*}P<0.002$ and $^{\&}P<0.002$ (Student's *t* test). CTR = control; ECAR = extracellular acidification rate; FCCP = trifluoromethoxy carbonylcyanide phenylhydrazone; QUCRC1 = ubiquinol-Cytochrome C reductase core protein 1.

differs from the one that promotes tumor progression. Given that mitochondrial dysfunction accompanies cardiovascular diseases (3, 25–29), it is of biological importance to characterize the mechanism underlying OLA1's mitochondrial protective function.

Here, we show that the post-translational form of OLA1 dictates its biological activity. When phosphorylated on T325, OLA1 effectively transforms into a transcription factor and translocates into the nucleus, enhancing the synthesis of nuclear-encoded mitochondrial proteins. Thus, our results indicate that phosphorylation-dependent OLA1 nuclear localization activates mitochondrial gene expression to promote cellular energy metabolism.

Methods

Details are provided in the data supplement.

Results

OLA1 Depletion Precipitates PPHN Vascular Phenotypes

OLA1 is expressed in mouse lung endothelial cells (MLECs) and mouse lung smooth muscle cells (Figure 1A; *see* Figure E1A in the data supplement). To examine the effects of OLA1 depletion on lung vascular development, we used an inducible OLA1$^{-/-}$ mouse model (*Endo*-OLA1$^{-/-}$). On Postnatal Day 7, *Endo*-OLA1$^{-/-}$ mice weighed less than wild-type (WT) mice (15–22 ± 6.2% [male] vs. 20–35 ± 1.9% [female]) (Figure 1B), suggesting that OLA1 might be required for fetuses to achieve their growth potential. Because growth retardation (intrauterine growth restriction) is an independent variable in PPHN pathobiology (30, 31), we compared right ventricular systolic pressure (RVSP) between WT and *Endo*-OLA1$^{-/-}$ mice. In WT OLA1 mice, RVSP was 19 ± 10 mm Hg, whereas in age- and sex-matched OLA1 knockout mice, it was 35–42 ± 12 mm Hg (Figure 1C). Although RVSP values varied among OLA1 knockout mice, they were consistently greater than 35 mm Hg. This variation could be due to the experimental approach used here (RVSP measurements were made on multiple days) but may also reflect the fact that pulmonary vascular resistance may vary among these mice. Nevertheless, it was

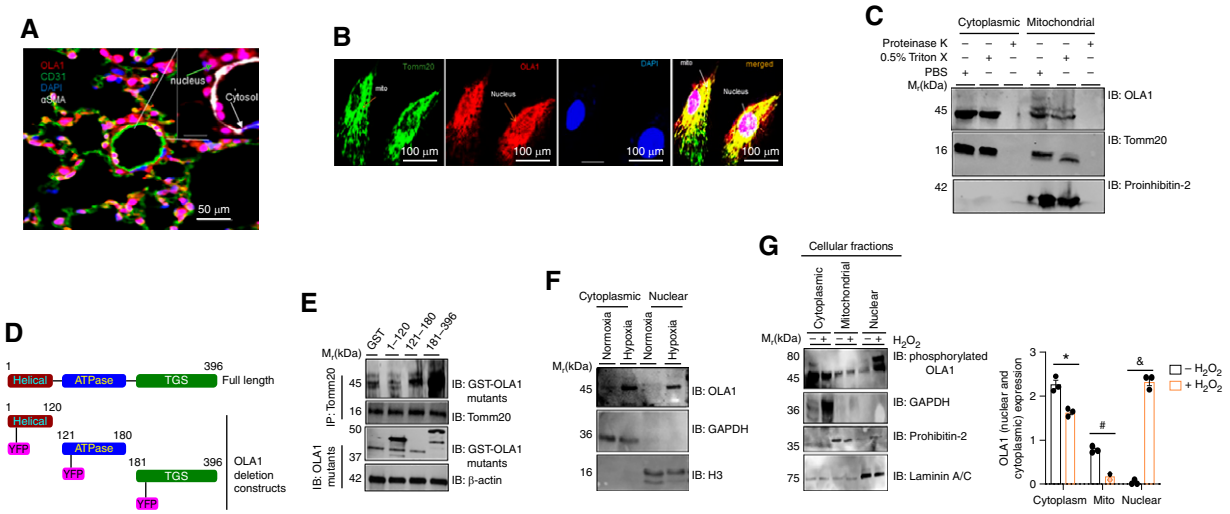

Figure 3. Cellular stress induces the translocation of OLA1 from cytoplasm/mitochondria (mito) into the nucleus. (*A*) Representative images of lung sections immunostained with anti-OLA1, anti-CD31, and anti-αSMA and counterstained with DAPI in mouse lung endothelial cells and smooth muscle cells in WT mouse lungs (scale bar, 50 μm; $n = 3$). (*B*) Representative images of PAECs immunostained with anti-OLA1 and anti-Tomm20 and counterstained with DAPI, showing the expression of OLA1 in the nucleus and mito under normal physiological conditions (scale bar, 100 μm; $n = 3$). (*C*) Representative images of OLA1 expression in the cytoplasm and mito isolated from PAECs after treatment with PBS, 0.5% Triton X-100 (SIGMA), or proteinase K (50 mg/ml) at 37°C for 10 minutes ($n = 4$). (*D*) Schematic illustration of glutathione S-transferase (GST)–tagged OLA1 domain deletion constructs on the basis of functional domains of the OLA1 protein. (*E*) Representative images showing the interactions between GST-tagged OLA1 domain deletion mutants and native Tomm20 protein. GST was used as the negative control, and β-actin was the loading control in whole-cell lysates ($n = 3$). (*F*) Representative images of OLA1 expression in the cytoplasmic and nuclear fractions obtained from normoxic PAECs and after exposure to 1% O_2 for 48 hours ($n = 4$). (*G*). Representative images of OLA1 expression in the cytosolic and nuclear fractions from PAECs at baseline and after treatment with 100 μm hydrogen peroxide (H_2O_2) for 1 hour. Laminin A/C or H3 and GAPDH were loading controls for the cytosolic and nuclear fractions. Bar charts represent densitometry quantifications in four biological replicates $^{*}P < 0.005$, $^{\#}P < 0.05$, and $^{\&}P < 0.05$ (Student's *t* test). H3 = histone 3; YFP = yellow fluorescent protein.

evident that OLA1 deletion in endothelial cells precipitated pulmonary hypertension after birth. Moreover, histological sections of *Endo*-OLA1$^{-/-}$ mouse lungs revealed muscularization and remodeling of normally nonmuscularized pulmonary arteries compared with male WT mice (Figure 1D). Histological sections of *Endo*-OLA1$^{-/-}$ hearts showed classic signs of right ventricular remodeling due to persistently elevated pulmonary vascular resistance (Figure 1E, upper panels), associated with some degree of cardiac fibrosis (Figure 1E, lower panels). Moreover, *Endo*-OLA1$^{-/-}$ lungs have decreased lung vascular density compared with those in WT mice (Figure 1F). Although MLECs from *Endo*-OLA1$^{-/-}$ mice were apoptotic and migrated less than those from WT mice (Figures 1G and 1H), mouse lung smooth muscle cells proliferated excessively *in vitro* (Figure 1I). These results suggest that OLA1 may be required for lung vascular development.

OLA1 Depletion Decreases Mitochondrial Function

Because decreases in mitochondrial biogenesis and function often accompany PPHN and other cardiovascular diseases (29–31), we proposed that OLA1 is essential for regulating mitochondrial stress responses during development. To this end, we compared the expression of select mitochondrial genes between WT and *Endo*-OLA1$^{-/-}$ mice. RT-qPCR analysis revealed decreased mRNA concentrations of nuclear-encoded mitochondrial proteins related to mitochondrial structure, protein complexes, and anion channels in Endo-OLA1$^{-/-}$ lungs relative to WT mice (Figure 2A). Furthermore, *Endo*-OLA1$^{-/-}$ lungs contain fewer mitochondria than WT mice (Figure 2B). In addition, the remaining mitochondria in MLECs from *Endo*-OLA1$^{-/-}$ lungs are structurally abnormal, with cystic dilatations and the absence of cristae and matrix proteins, whereas those in WT-MLECs appeared normal (Figure 2C). Accordingly, OLA1-depleted PAECs exhibited decreases in maximum respiratory capacity and ATP-linked oxygen consumption (Figure 2D), with an increase in extracellular acid production relative to control PAECs (Figure 2E). These results suggest a crucial role for OLA1 in maintaining mitochondrial content, structure, and function.

OLA1 Relocates into the Nucleus upon Cellular Stress

A closer examination of OLA1 subcellular localization revealed that OLA1 localizes in the cytoplasm and nucleus in lung cells (Figure 3A). Within the cytoplasm, OLA1 has a strong presence in mitochondria. Costaining with a mitochondrial marker, Tomm20 (translocase of outer mitochondrial membrane 20), showed that OLA1 localizes in the outer mitochondrial membrane (Figure 3B). The specificity of the immunostaining was confirmed by proteinase K assay. The digestion of the outer mitochondrial membrane by proteinase K for 20 minutes reduced the expression of OLA1 in mitochondria from PAECs (Figure 3C). Similarly, 0.5% Triton-X 100 (T9284, sigma) decreased the expression of OLA1 in the cytoplasm and mitochondria. This result, for the first time, identifies OLA1 as a mitochondrial protein. We validated this result using a series of OLA1 domain deletion constructs (Figure 3D). Protein–protein interaction analyses revealed

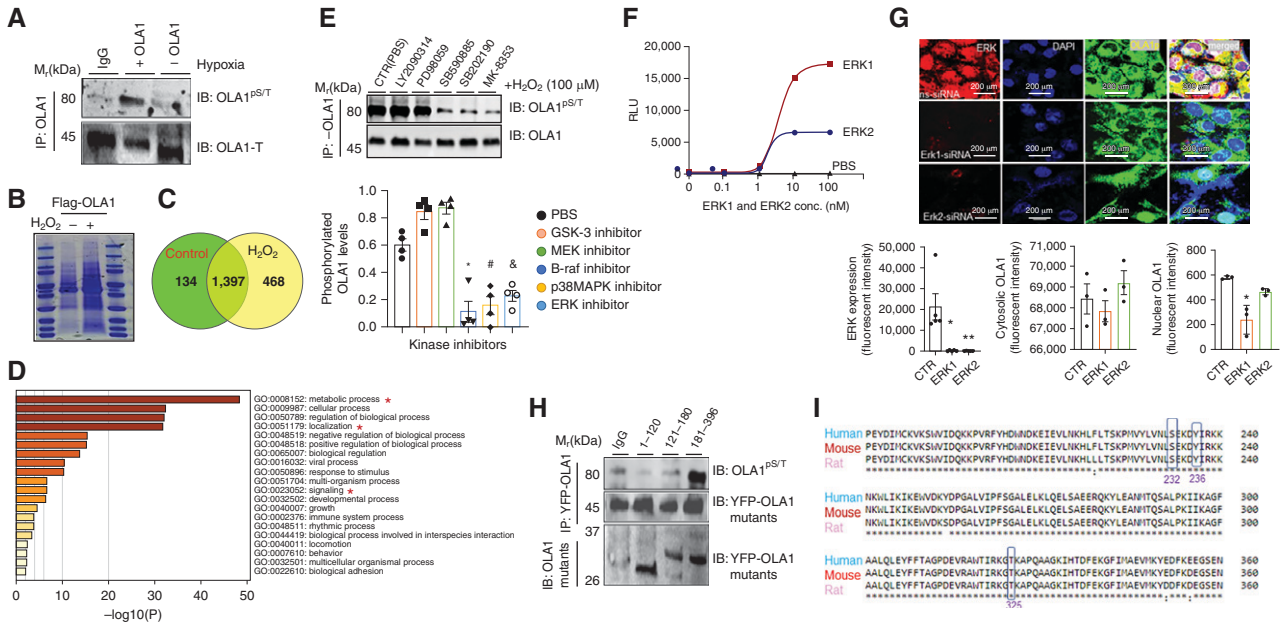

Figure 4. Phosphorylation triggers OLA1 nuclear localization. (*A*) Representative images of phosphorylated OLA1 expression in the cytoplasmic and nuclear fractions from MLECs under normoxic conditions and after exposure to acute hypoxia using a nonspecific pan-Ser/Thr antibody. (*B*) Representative gel images of Coomassie blue–stained gels of SDS PAGE–separated proteins derived from whole-cell lysates from PAECs and H_2O_2-treated PAECs ($n = 3$). (*C*) Venn diagram of OLA1 interacting partners in PAECs at baseline and after H_2O_2 treatment. (*D*) Gene Ontology term enrichment was analyzed using Metascape (http://metascape.org) software. The red asterisks denote pathways that associate with protein translocation. *P* values were calculated using hypergeometric tests. (*E*) Representative images showing phosphorylated OLA1 expression in whole-cell lysate from PAECs treated PBS or a series of kinase inhibitors and after H_2O_2 treatment ($n = 3$) $^{*}P < 0.0001$, $^{\#}P < 0.0001$, and $^{\&}P < 0.0001$ (two-way ANOVA). (*F*) Plots of enzyme kinetics of OLA1 protein phosphorylation by purified ERK1 (extracellular-regulated kinase 1) or ERK2 protein in an *in vitro* kinase reaction. The log of kinase concentrations was plotted against absorbance read at excitation/emission 540/590 nm with a 96-well plate reader ($n = 4$). Data are expressed as mean ± SEM, and two-way ANOVA was used to assess statistical significance. (*G*) Representative images of PAECs immunostained with anti-Flag antibodies and anti–ERK1/ERK2 antibodies and counterstained with DAPI in PAECs transfected Flag-OLA1$^{S232D\text{-}Y236E}$ mutant constructs after ERK1 or ERK2 was silenced using siRNA-mediated downregulation. The phosphomimetic OLA1 mutant was quantified in the cytoplasm and nucleus using Visiopharm 2.0 (http://visiopharm.com) software, and signal intensities were averages of three experiments. Scale bars = 200 μm. $^{*}P < 0.0001$ and $^{*}P < 0.0001$ (Student's *t* test). (*H*) Representative images of phosphorylated OLA1 in OLA1 domain deletion mutant constructs after treatment with H_2O_2. IgG was used as a control ($n = 5$). (*I*) Sequence alignments in OLA1 protein among humans, mice, and rats sequences using ClusterW2 (http://www.ebi.ac.uk) alignment software. GSK-3 = glycogen synthase kinase 3; MAPK = mitogen-activated protein kinase; MEK = MAPK/ERK kinase; RLU = relative light unit.

that OLA1 interacts with mitochondria via its C-terminal TGS domain (Figure 3E). Because analysis of the OLA1 sequence did not reveal any classic mitochondrial presequence (mitochondrial localization signal), our results suggest that the mitochondrial localization of OLA1 is likely driven by an internal mitochondrial localization signal located between amino acids (amino acids 181–396). Because OLA1 is also detected in the nucleus, we proposed that OLA1 translocates from mitochondria into the nucleus, where it promotes mitochondrial function during stress. To this end, we assessed OLA1 nuclear localization in response to stress using multiple stressors, including hypoxia (1% O_2 for 48 h), hydrogen peroxide (H_2O_2), and trifluoromethoxy carbonylcyanide phenylhydrazone. Not surprisingly, OLA1 accumulated in the nucleus of PAECs exposed to acute hypoxia (Figure 3F), trifluoromethoxy carbonylcyanide phenylhydrazone (*see* Figure E1B), and H_2O_2 treatment (Figure 3G). Concomitantly, the expression of OLA1 in the cytoplasm decreased, though less evidently in mitochondria, given their low yield in endothelial cells. Importantly, two distinct forms of OLA1 were detected in nuclear fractions from H_2O_2-treated cells, with one isoform having a molecular weight higher than the expected 45 kD for OLA1, suggesting that OLA1 may undergo post-translational modifications that drive its

Table 1. Extracellular-regulated Kinase 1 and Extracellular-regulated Kinase 2 Phosphorylation Sites in Human Obg-like ATPase-1 Protein

Kinase	Residue	Peptide
ERK1	224–238	PMVYLVNLSpEKDpYIR
ERK2	323–333	KGTKAPQAAGKR.KGTpKAPQAAGK.I

Definition of abbreviation: ERK = extracellular-regulated kinase.

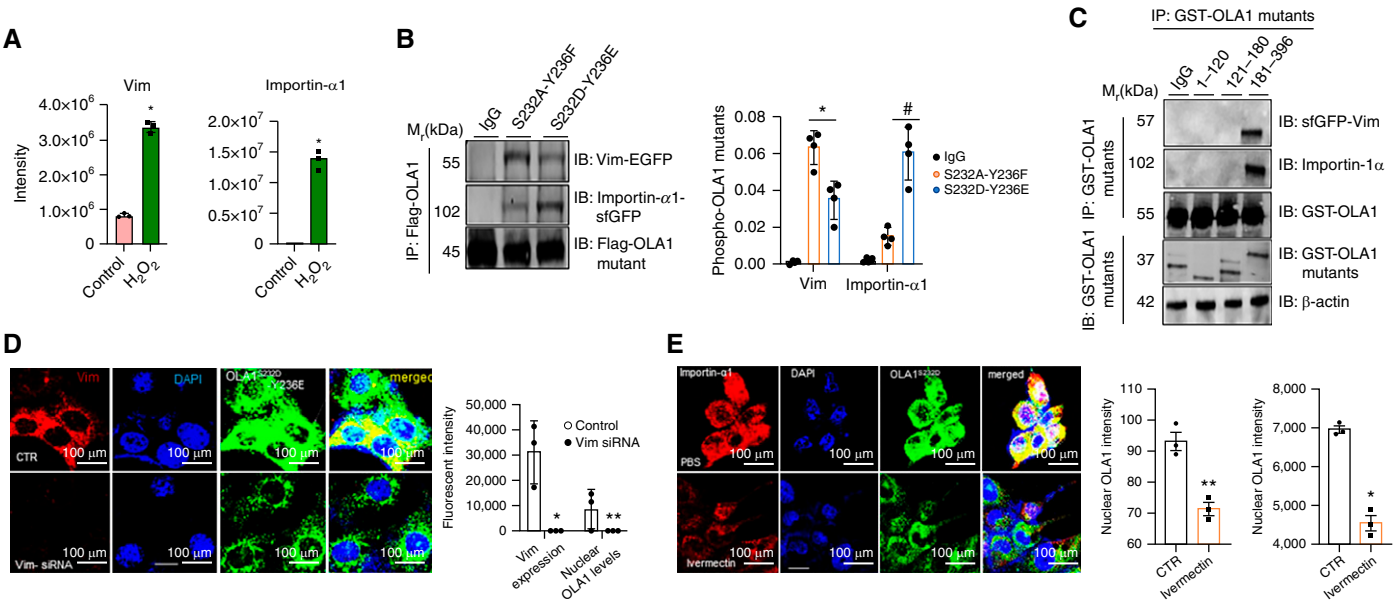

Figure 5. Vimentin (Vim) and importin-α1 cooperatively facilitate the nuclear translocation of phosphorylated OLA1. (*A*) Bar charts showing differences in OLA1 interactions with Vim and importin-1α assessed using mass spectrometry in PAECs with or without H_2O_2 treatment ($n = 3$). *$P < 0.002$ (Student's *t* test). (*B*) Representative images showing interactions between the phosphomimetic OLA1 (S232A-Y236F) or the phosphoresistant OLA1 (S232D-Y236E) mutant and superfolder GFP (sfGFP)–importin-α1 or enhanced GFP (EGFP)–Vim coexpressed in PAECs ($n = 3$). Data are expressed as mean ± SEM, and statistical significance was assessed using Student's *t* test ($n = 3$). *$P < 0.00013$ and #$P < 0.00013$ (one-WAY ANOVA). (*C*) Representative images showing interactions between OLA1 domain deletion constructs and sfGFP-Vim and EGFP-Vim after their coexpression in PAECs. IgG was the negative control. (*D*) Representative images of PAECs immunostained with anti-OLA1 showing changes in phosphorylated OLA1 expression in the nucleus at baseline and after Vim knocked down in PAECs with or without H_2O_2 treatment. Fixed cells were imaged at 63× magnification (scale bar, 100 μm). Fluorescent intensity was quantified, and values are plotted as bar charts ($n = 4$). *$P < 0.001$ (one-way ANOVA). (*E*) Representative images of PAECs immunostained with anti-OLA1 and counterstained with DAPI showing changes in the expression of phosphorylated OLA1 in the nucleus at baseline and after treatment of PAECs with IVE, which blocks importin-α, for 72 hours (scale bar, 100 μm). Signal intensity was quantified, and values are plotted as bar charts ($n = 4$). *$P < 0.001$ (Student's *t* test).

translocation into the nucleus. Together, these results indicate that cellular stress drives OLA1 nuclear localization.

Ser232/Tyr236 Phosphorylation Drives Nuclear OLA1 Translocation

To identify the post-translational modifications that modulate OLA1 function, we focused on phosphorylation, the most common modification in biology. Using a pan-Ser/Thr phosphorylation antibody, we found an increase in endogenous phosphorylation of OLA1 in PAECs exposed to acute hypoxia (Figure 4A). Similarly, H_2O_2 dose-dependently increased endogenous phosphorylation of OLA1 in PAECs (*see* Figure E1C). These results suggest that the increased molecular weight of OLA1 in the nucleus is likely due to phosphorylation. To identify the putative phosphorylation (sites), whole-cell lysate obtained from H_2O_2-treated or untreated PAECs was separated using SDS PAGE, Coomassie stained (Figure 4B), and analyzed using mass spectrometry for OLA1-specific kinase. Analysis revealed that OLA1 interacted with 468 more proteins in PAECs treated with H_2O_2 than untreated controls (Figure 4C). Gene Ontology analysis revealed that OLA1's partners are involved in diverse cellular processes, including subcellular localization, cell signaling, and stress responses (Figure 4D). Proteomic screens identified ERKs, MAPK (mitogen-activated protein kinase), GSK3 (glycogen synthase kinase 3), and CDKs (cyclin-dependent kinases) as top hits, validated by co-IP (*see* Figures E1D and E1E). To determine the kinase specific to OLA1, we performed a kinase inhibition assay, finding that inhibition of B-Raf, MAPK, or ERK1/2—but not CDK or GSK3—decreased endogenous phosphorylation of OLA1 (Figure 4E). This result suggests that ERK may be one of the OLA1-specific kinases. The specificity of OLA1 phosphorylation by ERK1 or ERK2 in PAECs was further assessed using *in vitro* kinase assays (Figure 4F) and confirmed by ERK1 or ERK2 downregulation using siRNA (*see* Figure E2A). Although *in silico* prediction analysis using NetPhos 2.0 (http://www.cbs.dtu.dk/sevices/NetPhos/) did not identify ERK as an OLA1 kinase, our results indicate that ERK may be a physiological kinase for OLA1 (*see* Figure E2B). To pinpoint ERK phosphorylation site(s), we performed a phosphoproteomics screen, which revealed that ERK1 phosphorylated Ser(S232) and Tyr(Y236), while ERK2 phosphorylated Thr(T325) in OLA1 protein (*see* Figures E2C and E2D; Table 1). Custom antibodies raised against phosphorylated S232, Y236, or T325-OLA1 could detect OLA1 phosphorylation in phosphomimetic OLA1 mutants but not in the phosphoresistant OLA1 mutant (*see* Figure E3A).

Because OLA1 is extensively phosphorylated, we examined the impact of phosphorylation on nuclear localization. PAECs were transfected with Flag-tagged OLA1 mutants mimicking native and phosphorylated states. Cells expressing phosphoresistant OLA1 mutants (S232A-Y236F) had negligible OLA1 in the nucleus,

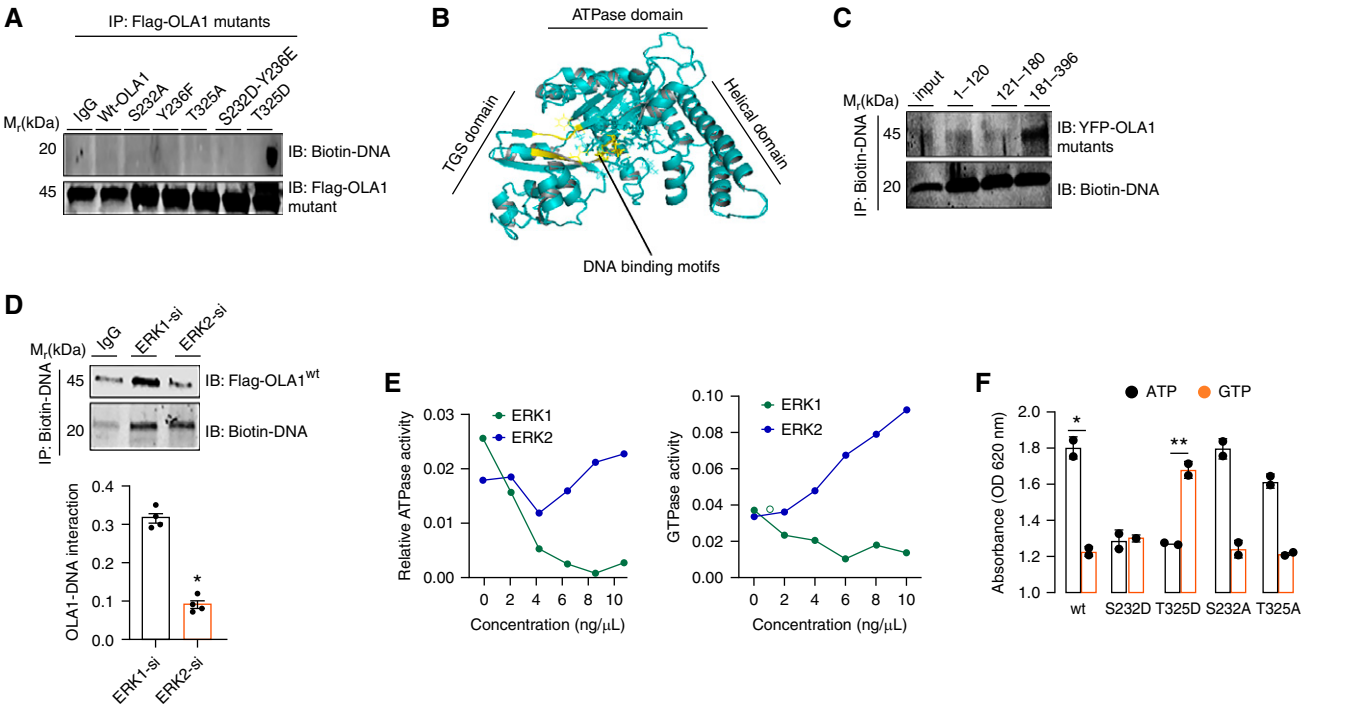

Figure 6. T325 phosphorylation enhances OLA1 binding to DNA. (*A*) Representative images showing interactions between immunopurified WT OLA1, mutant OLA1 (WT, S232D, Y232F, T325A, T325D, and S232D-Y236E), and biotinylated nuclear DNA obtained from PAECs. OLA1-DNA binding was analyzed using IP and IB analyses ($n = 3$). IgG was used as the control. (*B*) Crystallographic analysis of DNA-binding motifs in human OLA1 protein with I-TASSER using existing crystallographic data (Protein Data Bank: 2OHF). (*C*) Representative images of the interaction between OLA1 domain deletion constructs and biotinylated DNA. (*D*) Interactions between immunopurified OLA1 proteins from ERK1- or ERK2-silenced PAECs and biotin-labeled genomic DNA. Bar charts represent the results ($n = 5$). *$P < 0.005$ (one-way ANOVA). (*E*) Graphs of ATP hydrolysis by purified OLA1 protein phosphorylated by ERK1 on Ser232/Y236 or ERK2 on T325. (*F*) Graphs of GTP hydrolysis by purified OLA1 protein phosphorylated by ERK1 or ERK2. Absorbance read at 620 nm with a plate reader was corrected against protein concentration ($n = 4$). *$P < 0.00001$ and **$P < 0.00001$. Data are expressed as mean ± SEM, and two-way ANOVA was used to assess statistical significance.

even in the presence of H_2O_2. Except for $OLA1^{T325D}$, the phosphomimetic OLA1 mutants (S232D-Y236E) accumulated in the nucleus without H_2O_2. Upon H_2O_2 treatment, however, the $OLA1^{T325D}$ mutant accumulated in the nucleus (*see* Figure E3B), suggesting that phosphorylation of S232 or Y236 is required for OLA1's nuclear translocation. Moreover, silencing ERK1 (which phosphorylates S232/Y236) blocked the nuclear accumulation of Flag-$OLA1^{S232D}$ mutant in the presence of H_2O_2 (Figure 4G); conversely, silencing ERK2 (which phosphorylates T325) increased nuclear OLA1 expression (*see* Figure E3C), suggesting that T325 phosphorylation is not required for nuclear translocation. Furthermore, C-terminal deletion abolished OLA1 phosphorylation (Figure 4H). Although we did not expect the silencing of ERK1 or ERK2 to decrease total ERK concentrations, the reciprocal effect of ERK1 and ERK2 depletion on the nuclear OLA1 accumulation demonstrates the specificity of each siRNA and the biological effect of each ERK isoform in regulating OLA1 activity. Collectively, these results suggest that OLA1 phosphorylation on S232/Y236 by ERK1 controls its nuclear translocation. Furthermore, the evolutionarily conserved nature of S232/Y236/T325 residues in humans, mice, and rats attests to the importance of these residues in the OLA1 function (Figure 4I).

The Nucleocytoplasmic System Facilitates Nuclear OLA1 Translocation

We then wondered how OLA1 is translocated into the nucleus upon phosphorylation. Our proteomic data revealed that OLA1 interacts with several cytoskeletal proteins, including Vim (vimentin) and KPNA2 (karyopherin subunit alpha 2) (importin-α1) in PAECs, and we validated this finding with co-IP (Figure 5A; *see* Figure E4A). On the basis of publications (32–34) on the essential role of the nucleocytoplasmic system in the nuclear localization of proteins and our proteomic data, we hypothesized that Vim and importin-α1 are involved in OLA1 nuclear localization. Moreover, there is evidence indicating that Vim prevents mitochondrial damage during stress (33). To test this hypothesis, we examined the relationship between Vim and OLA1, finding that Vim interacted with phosphoresistant and phosphomimetic OLA1 mutants (Figure 5B). Specifically, Vim is bound to OLA1 through its C-terminal TGS domain (Figure 5C). Knocking Vim down using siRNA abolished the nuclear translocation of phosphorylated OLA1 (Figure 5D), suggesting that Vim regulates mitochondrial function partly by promoting the nuclear localization of OLA1. Like Vim, importin-α1 also interacted with OLA1. But unlike Vim, importin-α1 is bound to phosphomimetic OLA1 mutants more than phosphoresistant mutants (Figure 5B), suggesting that importin-α1 interacts more with phosphorylated OLA1. To examine the relationship between OLA1 and importin-α1 in the context of OLA1 nuclear localization, we used IVE, an

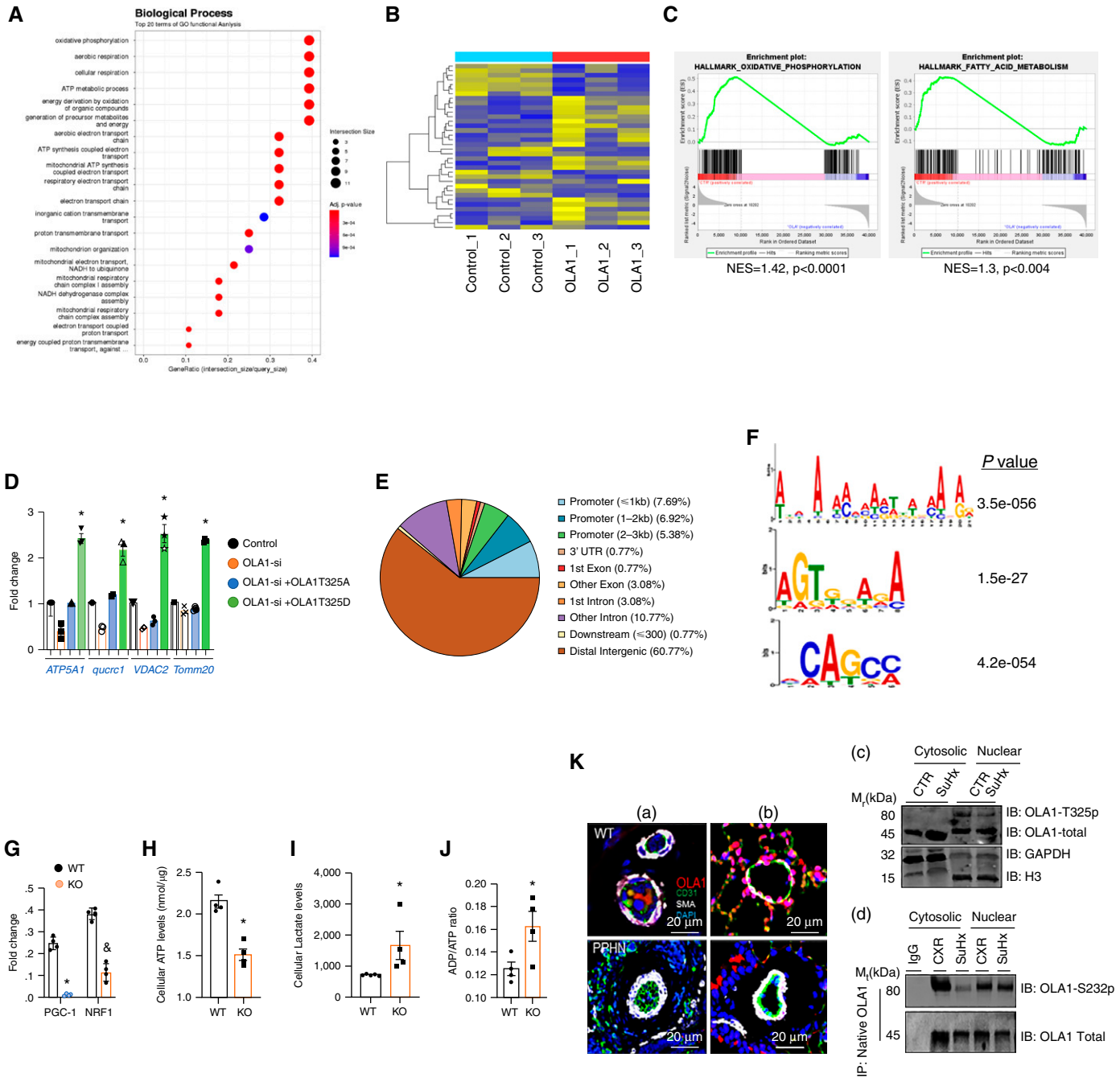

Figure 7. Nuclear OLA1 regulates gene expression. Total RNA extracted from OLA1-depleted PAECs and parental cells (as controls) was sequenced. (*A*) Gene Ontology term enrichment was analyzed using Metascape software. The top 20 terms relating to downregulated mitochondrial functions are indicated in red. Dot size indicates fold enrichment. Statistical analysis was performed using modified Fisher exact tests with Benjamini-Hochberg correction. (*B*) Heat maps of the differentially expressed genes in OLA1-depleted and parental PAECs. (*C*) Downregulated gene-set enrichment analysis signatures in OLA1-depleted PAECs. *P* values were calculated using Kolmogorov-Smirnov tests. (*D*) RT-qPCR analysis of nuclear-encoded mitochondrial proteins (nuclear-encoded mitochondrial genes) in control PAECs and OLA1-depleted PAECs, or in OLA1-depleted PAECs transfected with OLA1 attached to nuclear localizing sequence, or to nuclear-excluded sequence ($n = 3$). $^{*}P < 0.0001$ (Student's *t* test). (*E*) Genomic distribution of red fluorescent protein (RFP)-tag chromatin IP with high-throughput DNA sequencing peaks in OLA1-depleted cells expressing RFP-OLA1^{T325D}. (*F*) The top enriched motifs in the OLA1-binding sites in PAECs ($n = 2$). *P* values were calculated using hypergeometric distributions. (*G*) Bar charts of NRF1 (nuclear respiratory factor 1) and PGC-1α (PPARG coactivator 1α) mRNA concentrations in WT mice and Endo-OLA1 KO lungs (male) killed on Postnatal Day 10. Data are represented as mean ± SEM of fold change and assessed using Student's *t* test. Actin was used as loading control ($n = 4$). $^{*}P < 0.0023$ and $^{\&}P < 0.0023$. (*H–J*) Bar charts of total cellular ATP concentrations (*H*), lactate concentrations (*I*), and ADP:ATP ratios (*J*) in MLECs isolated from WT and

inhibitor of importin α/β, finding that blocking importin-α1 interaction abolished the translocation of phosphorylated OLA1 into the nucleus (Figure 5E). Mechanistically, OLA1 interacted with importin-α1 via its C-terminal domain (Figure 5C). These results indicate that Vim and importin-α1 regulate mitochondrial function by facilitating the nuclear localization of OLA1. Hence, we propose a new paradigm for a retrograde mitonuclear communication pathway in which, under normal physiological conditions, OLA1 resides on mitochondria anchored by Vim. However, OLA1 becomes phosphorylated upon stress, disengages from mitochondria, and relocates into the nucleus by interacting with Vim and importin-α1.

Nuclear OLA1 Regulates Mitochondrial Gene Expression

Our findings suggest that the function of OLA1 may involve interactions with nuclear DNA. Protein–DNA interaction assays indicated that OLA1 binds to DNA *in vitro*. This DNA binding is potentiated by T325 phosphorylation (Figure 6A). Molecular modeling using I-TASSER (35) in WT OLA1 and mutant OLA1 after T-to-A mutation revealed that T325 phosphorylation induced structural changes in OLA1 protein that exposed DNA-binding motifs, which were otherwise buried within the protein core in the unphosphorylated form (Figure 6B; *see* Figure E4B). The regulatory role of T325 phosphorylation on DNA binding was confirmed by C-terminal deletion (amino acids 181–396), and ERK2-siRNA–mediated downregulation, which abolished the binding of OLA1 to DNA (Figures 6C and 6D). In addition, biochemical analysis of OLA1 activity revealed that T325 phosphorylation increases the GTPase activity of OLA1 while suppressing its ATPase activity (Figures 6E and 6F). These results suggest that OLA1 binds to DNA via its C-terminal residues, which undergo phosphorylation and display high GTPase activity.

OLA1 Regulates the Expression of Genes Linked to Mitochondrial Energy Metabolism

To determine the physiological significance of OLA1 interaction with DNA, we performed RNA sequencing, comparing gene expression profiles between control PAECs and OLA1-depleted PAECs. Interestingly, OLA1 depletion in PAECs downregulated a panel of genes involved in oxidative phosphorylation pathways, mitochondrial assembly, and structure (Figures 7A–7C). The oxidative phosphorylation category is the topmost enriched functional group in OLA1-depleted PAECs. In addition, OLA1 depletion decreased the expression of nuclear-encoded mitochondrial proteins. Reintroducing a phosphomimetic OLA1^{T325D} mutant fused to a nuclear localizing sequence but not the phosphoresistant OLA1^{T325A} mutant rescues the expression of the downregulated mitochondrial genes in OLA1-depleted PAECs (Figures 7D–7F). This result supports that OLA1 localizes in the nucleus to affect mitochondrial gene transcription.

To further dissect the function of OLA1 in mitochondrial gene expression, we performed chromatin IP with high-throughput DNA sequencing analysis using OLA1-silenced PAECs in which we reintroduced red fluorescent protein (RFP)–tagged nuclear localizing sequence OLA1^{T325D}. We observed an overlap between OLA1 chromatin IP with high-throughput DNA sequencing genes and differentially expressed genes in OLA1-silenced cells. In addition, we identified a subset of *de novo* OLA1-binding motifs and canonical binding motifs of various transcription factors (Figures 7G and 7H; see Table E1). Comparing the DNA patterns with other transcription factors, we found a positive correlation with transcription factors regulating mitochondrial biogenesis, including NRF1 (nuclear respiratory factor 1), PGC-1α (PPARG coactivator 1α), and others. These data suggest that OLA1 may affect the function of these factors. Indeed, the expression of PGC-1α and NRF1 expression was downregulated in *Endo*-OLA1$^{-/-}$ lungs (Figure 7G), suggesting that the decreased mitochondrial function in *Endo*-OLA1$^{-/-}$ is caused by the downregulation of multiple metabolic genes. This conclusion is supported by decreased total cellular ATP concentrations and increased lactate concentrations in MLECs isolated from *Endo*-OLA1$^{-/-}$ lungs (Figures 7H and 7I). Interestingly, *Endo*-OLA1$^{-/-}$ lungs have a higher ADP:ATP ratio than WT mice (Figure 7J), suggesting increased ATP use or disruption of ATP synthesis. Although a rise in ADP:ATP ratio in healthy lungs is a physiological cue to restore energy homeostasis (36), the sustained increase in ADP:ATP ratio without an increase in ATP concentrations strongly suggests impaired mitochondrial energy production due to decreased expression of NRF1 and PGC-1α genes by OLA1 depletion. These results support a crucial role for OLA1 in cellular energy metabolism and identified OLA1 deficiency as a factor in mitochondrial dysfunction in PPHN.

PP1A Prevents Overactivation of OLA1 Transcriptional Activity

Next, we investigated how OLA1 activation is terminated once stress abates. As phosphorylation enhances the GTPase activity and DNA binding of OLA1, we focused on Ser/Thr phosphatases (PPAs [protein phosphatases]). Our mass spectrometry data revealed that OLA1 interacts with PP1A, a ubiquitously expressed Ser/Thr protein phosphatase, and UBA52 (ubiquitin A-52 residue ribosomal protein fusion product 1), an E3 ubiquitin ligase. UBA52 and PP1A coimmunoprecipitated with the phosphomimetic and phosphoresistant OLA1 mutants (*see* Figures E4C and E4D). To examine the relationship between PP1A and UBA52 in the context of OLA1 activity, we performed *in vitro* ubiquitination assays. WT OLA1 was substantially

Figure 7. (*Continued*). Endo-OLA1$^{-/-}$ mice using liquid chromatography–tandem mass spectrometry ($n = 4$). *$P < 0.0001$ (Student's *t* test). (*Ka* and *Kb*) Representative images of lung sections immunostained with anti-OLA1, anti-CD31, and anti-αSMA and counterstained with DAPI in patients with persistent pulmonary hypertension of the newborn (PPHN): (*Ka*) hypoxia/Sugen (SuHx) PPHN mice and normoxic control animals and (*Kb*) patients with PPHN and age-matched control subjects. (*Kc*) Representative images of OLA1 expression (nonphosphorylated in the cytoplasmic fraction and phosphorylated OLA1-T325 in the nuclear fractions from WT mice and SuHx mouse lungs killed after chronic hypoxia and treated with Sugen 5416 20 mg/kg, intraperitoneal, weekly for 3 weeks. (*Kd*) Representative images showing expression of phosphorylated OLA1-S232 in the cytosolic and nuclear fractions from WT mice and SuHx PPHN mouse lungs ($n = 3$). Scale bars, 20 μm. CXR = control; NADH = NAD$^+$ reduced; NES = normalized enrichment score; SuHx = hypoxia/Sugen; UTR = untranslated region.

ubiquitinated by UBA52. Conversely, phosphorylated OLA1 mutants were resistant to UBA52-mediated ubiquitination of OLA1. When active PP1A enzyme was added to *in vitro* reactions between OLA1 and ERK, phosphorylated OLA1 became significantly ubiquitinated (*see* Figures E4E and E4F). These results support the idea that PP1A and UBA52 cooperatively terminate OLA1 activation via dephosphorylation and ubiquitin-mediated degradation.

OLA1 Phosphorylation Is Decreased in Patients with PPHN and Hypoxia/Sugen Mice

To establish a connection between OLA1^{T325} phosphorylation and PPHN, we used human lung samples, comparing OLA1^{pT325} concentrations in the nucleus between infants who died of PPHN and age-matched control subjects. IF analysis revealed decreased nuclear OLA1(pT325) concentrations in the remodeled PPHN pulmonary arteries compared with control subjects (Figure 7K; *see* Figure E5A). We validated this result using hypoxia/Sugen mice, finding increased expression of OLA1 in the cytosolic fractions from hypoxia/Sugen lungs (Figure 7Kb). Despite this increase, the concentrations of S232-phosphorylated OLA1 and T325-phosphorylated OLA1 were decreased in the cytoplasm and nucleus, respectively (Figure 7Kc) in parallel to increases in the expression of PP1A and UBA52, both of which are targets of OLA1 (*see* Figure E5B). These changes led to an increase in ubiquitinated OLA1 protein concentrations and a decrease in total OLA1 concentrations (*see* Figure E5C), suggesting enhanced degradation of OLA1 and supporting the idea that altered kinase–phosphatase balance induced by chronic hypoxia contributes to OLA1 insufficiency and PPHN progression.

These findings suggest a new mitonuclear retrograde communication model that underlies how OLA1 expression correlates with endothelial mitochondrial function during stress. First, highly expressed ERK kinases engage OLA1 in mitochondria to promote its nuclear translocation; second, OLA1 in the nucleus enhances the activation of multiple mitochondrial genes to increase cellular energy metabolism, critical cell survival, and function during stress.

Discussion

The stress protein OLA1 has been implicated in multiple processes regulating the cellular stress response (20, 21, 37). Previous studies have focused on OLA1 roles at the post-transcriptional level, but we report here that OLA1 also regulates gene expression. We demonstrated that OLA1 is an essential component of the mitonuclear regulator hubs that link mitochondrial redox control mechanisms to metabolic gene networks in the nucleus. We found that OLA1, which typically resides in mitochondria and cytoplasm, relocates into the nucleus when phosphorylated in response to oxidative and metabolic stresses. Subsequent phosphorylation of nuclear OLA1 on T325 prompts it to turn on a cohort of genes relevant to mitochondrial function and cellular adaptation to stress. Once the stress abates, PPIA and UBA52 converge on phosphorylated OLA1, dephosphorylating and targeting it for proteasomal degradation. Thus, turning off OLA1-mediated gene expression to restore cellular homeostasis. Our findings *in vitro*, in cells, and in laboratory animals reveal OLA1 as a target in modulating mitochondrial function.

Our data explain why altered ERK-OLA1 signaling contributes to mitochondrial dysfunction underpinning PPHN. We demonstrated that the concentration of OLA1pT325 in the nucleus closely correlates with mitochondrial content and function in the vascular endothelium. Given that ERK controls OLA1 nuclear localization, and PP1A activation counteracts this process, altered PP1A-OLA1 signaling might conceivably be a key player in mitochondrial dysfunction in PPHN. However, essential questions remain regarding how OLA1 regulates NRF1 and PGC-1α function.

Although PPHN behaves similarly to cancer (though it does not metastasize), our results highlight apparent differences in stress response in these two conditions. PP1A and ubiquitin ligases are genetically downregulated in many tumors (38, 39), allowing unhindered OLA1-mediated expression of stress response genes. We speculate that this effect could expand cancer cell subpopulations adept at resisting stress and promote recovery from stress induced by chemotherapeutic agents. In support of this notion, many studies have demonstrated that higher OLA1 expression promotes tumor progression and chemoresistance. Conversely, PP1 and ubiquitin ligases are overexpressed in vascular diseases, disrupting the nuclear OLA1 localization and inhibiting mitochondrial gene expression, thereby sensitizing vascular cells to cellular damage and dysfunction. ■

Author disclosures are available with the text of this article at www.atsjournals.org.

References

1. Agarwal S, Ganesh S. Perinuclear mitochondrial clustering, increased ROS levels, and HIF1 are required for the activation of HSF1 by heat stress. *J Cell Sci* 2020;133:jcs245589.
2. An H, Zhou B, Ji X. Mitochondrial quality control in acute ischemic stroke. *J Cereb Blood Flow Metab* 2021;41:3157–3170.
3. Andréasson C, Ott M, Büttner S. Mitochondria orchestrate proteostatic and metabolic stress responses. *EMBO Rep* 2019;20:e47865.
4. Bermejo-Nogales A, Nederlof M, Benedito-Palos L, Ballester-Lozano GF, Folkedal O, Olsen RE, *et al.* Metabolic and transcriptional responses of gilthead sea bream (*Sparus aurata* L.) to environmental stress: new insights in fish mitochondrial phenotyping. *Gen Comp Endocrinol* 2014; 205:305–315.
5. Broadley SA, Hartl FU. Mitochondrial stress signaling: a pathway unfolds. *Trends Cell Biol* 2008;18:1–4.
6. Cardamone MD, Tanasa B, Cederquist CT, Huang J, Mahdaviani K, Li W, *et al.* Mitochondrial retrograde signaling in mammals is mediated by the transcriptional cofactor GPS2 via direct mitochondria-to-nucleus translocation. *Mol Cell* 2018;69:757–772.e7.
7. Alam F, Syed H, Amjad S, Baig M, Khan TA, Rehman R. Interplay between oxidative stress, SIRT1, reproductive and metabolic functions. *Curr Res Physiol* 2021;4:119–124.
8. Ande SR, Mishra S. Nuclear coded mitochondrial protein prohibitin is an iron regulated iron binding protein. *Mitochondrion* 2011;11:40–47.
9. Cheng Z, Völkers M, Din S, Avitabile D, Khan M, Gude N, *et al.* Mitochondrial translocation of Nur77 mediates cardiomyocyte apoptosis. *Eur Heart J* 2011;32:2179–2188.

10. Arnould T, Michel S, Renard P. Mitochondria retrograde signaling and the UPR mt: where are we in mammals? *Int J Mol Sci* 2015;16: 18224–18251.
11. Wu X, Xu T, Li D, Zhu S, Chen Q, Hu W, *et al.* ERK/PP1a/PLB/ SERCA2a and JNK pathways are involved in luteolin-mediated protection of rat hearts and cardiomyocytes following ischemia/ reperfusion. *PLoS One* 2013;8:e82957.
12. Zhang LJ, Chen S, Wu P, Hu CS, Thorne RF, Luo CM, *et al.* Inhibition of MEK blocks GRP78 up-regulation and enhances apoptosis induced by ER stress in gastric cancer cells. *Cancer Lett* 2009;274:40–46.
13. Huang CF, Liu SH, Su CC, Fang KM, Yen CC, Yang CY, *et al.* Roles of ERK/Akt signals in mitochondria-dependent and endoplasmic reticulum stress-triggered neuronal cell apoptosis induced by 4-methyl-2,4-bis(4-hydroxyphenyl)pent-1-ene, a major active metabolite of bisphenol A. *Toxicology* 2021;455:152764.
14. Sauer F, Riou M, Charles AL, Meyer A, Andres E, Geny B, *et al.* Pathophysiology of heart failure: a role for peripheral blood mononuclear cells mitochondrial dysfunction? *J Clin Med* 2022;11:741.
15. Wenk M, Ba Q, Erichsen V, MacInnes K, Wiese H, Warscheid B, *et al.* A universally conserved ATPase regulates the oxidative stress response in *Escherichia coli*. *J Biol Chem* 2012;287:43585–43598.
16. Schultz A, Olorundami OA, Teng RJ, Jarzembowski J, Shi ZZ, Kumar SN, *et al.* Decreased OLA1 (Obg-like ATPase-1) expression drives ubiquitin-proteasome pathways to downregulate mitochondrial SOD2 (superoxide dismutase) in persistent pulmonary hypertension of the newborn. *Hypertension* 2019;74:957–966.
17. Chen H, Song R, Wang G, Ding Z, Yang C, Zhang J, *et al.* OLA1 regulates protein synthesis and integrated stress response by inhibiting eIF2 ternary complex formation. *Sci Rep* 2015;5:13241.
18. Zhang J, Rubio V, Lieberman MW, Shi ZZ. OLA1, an Obg-like ATPase, suppresses antioxidant response via nontranscriptional mechanisms. *Proc Natl Acad Sci USA* 2009;106:15356–15361.
19. Zemanovic S, Ivanov MV, Ivanova LV, Bhatnagar A, Michalkiewicz T, Teng RJ, *et al.* Dynamic phosphorylation of the C terminus of Hsp70 regulates the mitochondrial import of SOD2 and redox balance. *Cell Rep* 2018;25:2605–2616.e7.
20. Mao RF, Rubio V, Chen H, Bai L, Mansour OC, Shi ZZ. OLA1 protects cells in heat shock by stabilizing HSP70. *Cell Death Dis* 2013;4:e491.
21. Dannenmaier S, Desroches Altamirano C, Schüler L, Zhang Y, Hummel J, Milanov M, *et al.* Quantitative proteomics identifies the universally conserved ATPase Ola1p as a positive regulator of heat shock response in *Saccharomyces cerevisiae*. *J Biol Chem* 2021; 297:101050.
22. Ding Z, Liu Y, Rubio V, He J, Minze LJ, Shi ZZ. OLA1, a translational regulator of p21, maintains optimal cell proliferation necessary for developmental progression. *Mol Cell Biol* 2016;36:2568–2582.
23. Dong Y, Yin A, Xu C, Jiang H, Wang Q, Wu W, *et al.* OLA1 is a potential prognostic molecular biomarker for endometrial cancer and promotes tumor progression. *Oncol Lett* 2021;22:576.
24. Huang S, Zhang C, Sun C, Hou Y, Zhang Y, Tam NL, *et al.* Obg-like ATPase 1 (OLA1) overexpression predicts poor prognosis and promotes tumor progression by regulating P21/CDK2 in hepatocellular carcinoma. *Aging (Albany NY)* 2020;12:3025–3041.
25. Ashrafizadeh M, Mirzaei S, Hushmandi K, Rahmanian V, Zabolian A, Raei M, *et al.* Therapeutic potential of AMPK signaling targeting in lung cancer: advances, challenges and future prospects. *Life Sci* 2021;278: 119649.
26. Cano M, Datta S, Wang L, Liu T, Flores-Bellver M, Sachdeva M, *et al.* Nrf2 deficiency decreases NADPH from impaired IDH shuttle and pentose phosphate pathway in retinal pigmented epithelial cells to magnify oxidative stress-induced mitochondrial dysfunction. *Aging Cell* 2021;20:e13444.
27. Chan SY, Rubin LJ. Metabolic dysfunction in pulmonary hypertension: from basic science to clinical practice. *Eur Respir Rev* 2017; 26:170094.
28. Kaboli PJ, Imani S, Jomhori M, Ling KH. Chemoresistance in breast cancer: PI3K/Akt pathway inhibitors vs the current chemotherapy. *Am J Cancer Res* 2021;11:5155–5183.
29. Sharma M, Rana U, Joshi C, Michalkiewicz T, Afolayan A, Parchur A, *et al.* Decreased cyclic guanosine monophosphate-protein kinase G signaling impairs angiogenesis in a lamb model of persistent pulmonary hypertension of the newborn. *Am J Respir Cell Mol Biol* 2021;65: 555–567.
30. Pels A, Onland W, Berger RMF, van Heijst AFJ, Lopriore E, Reiss IKM, *et al.* Neonatal pulmonary hypertension after severe early-onset fetal growth restriction: post hoc reflections on the Dutch STRIDER study. *Eur J Pediatr* 2022;181:1709–1718.
31. Rosenberg A. The IUGR newborn. *Semin Perinatol* 2008;32: 219–224.
32. Li Y, Huang Y, Ren S, Xiao X, Cao H, He J. A pan-cancer analysis of the oncogenic role of nuclear transport factor 2 in human cancers. *Front Oncol* 2022;12:829389.
33. Pan P, Su L, Wang X, Chai W, Liu D, Song L, *et al.* Vimentin regulation of autophagy activation in lung fibroblasts in response to lipopolysaccharide exposure in vitro. *Ann Transl Med* 2021;9:304.
34. de Pablo Y, Marasek P, Pozo-Rodrigálvarez A, Wilhelmsson U, Inagaki M, Pekna M, *et al.* Vimentin phosphorylation is required for normal cell division of immature astrocytes. *Cells* 2019;8:1016.
35. Roy A, Kucukural A, Zhang Y. I-TASSER: a unified platform for automated protein structure and function prediction. *Nat Protoc* 2010;5: 725–738.
36. Rana U, Callan E, Entringer B, Michalkiewicz T, Joshi A, Parchur AK, *et al.* AMP-kinase dysfunction alters notch ligands to impair angiogenesis in neonatal pulmonary hypertension. *Am J Respir Cell Mol Biol* 2020;62:719–731.
37. Hannemann L, Suppanz I, Ba Q, MacInnes K, Drepper F, Warscheid B, *et al.* Redox activation of the universally conserved ATPase YchF by thioredoxin 1. *Antioxid Redox Signal* 2016;24:141–156.
38. Luo Z, Ye X, Cheng Y, Li F, Shou F, Wang G. E3 ubiquitin ligase PJA1 regulates lung adenocarcinoma apoptosis and invasion through promoting FOXR2 degradation. *Biochem Biophys Res Commun* 2021; 556:106–113.
39. Ferrer I, Verdugo-Sivianes EM, Castilla MA, Melendez R, Marin JJ, Muñoz-Galvan S, *et al.* Loss of the tumor suppressor spinophilin (PPP1R9B) increases the cancer stem cell population in breast tumors. *Oncogene* 2016;35:2777–2788.